Wiley
International Journal of Energy Research
Volume 2025, Article ID 6738352, 11 pages
https://doi.org/10.1155/er/6738352

WILEY

Research Article

Highly Stable and Rechargeable Lithium-Ion Battery Using a Designed Organic PTVE-Impregnated Porous Graphitic Carbon Composite

Ji-Won Son,[1] Jae Seob Lee,[1,2] Hyun Ho Choi,[1] Fanglin Wu,[3] Hong-Il Kim,[4] Tae Ju Kang,[4] Hyun Woo Kim,[5] Shan Fang,[6] Ying Liu,[4] and Jung Sang Cho[1,7,8]

[1]*Department of Engineering Chemistry, Chungbuk National University, Cheongju 28644, Chungbuk, Republic of Korea*
[2]*Department of Materials Science and Engineering, Korea University, Anam-Dong, Seongbuk-Gu, Seoul 02841, Republic of Korea*
[3]*State Key Laboratory of Advanced Technology for Materials Synthesis and Processing, Wuhan University of Technology, Wuhan 430070, China*
[4]*Department of Energy Convergence Engineering, Cheongju University, 285 Daeseong-ro, Cheongju 28503, Chungbuk, Republic of Korea*
[5]*Department of Chemical Engineering, Gyeongsang National University, Jinju 52828, Republic of Korea*
[6]*School of Physics and Materials, Nanchang University, Nanchang 330031, Jiangxi, China*
[7]*Biomedical Research Institute, Chungbuk National University Hospital, 361-763, Cheongju 28644, Chungbuk, Republic of Korea*
[8]*Advanced Energy Research Institute, Chungbuk National University, Cheongju 28644, Chungbuk, Republic of Korea*

Correspondence should be addressed to Fanglin Wu; fanglin-wu@whut.edu.cn, Hyun Woo Kim; khw5536@gnu.ac.kr, and Jung Sang Cho; jscho@chungbuk.ac.kr

Received 20 November 2024; Accepted 22 April 2025

Academic Editor: Amar Patil

Organic rechargeable batteries have the advantages of environmental friendliness, effortless availability, rapid charging ability, and high-power output. However, organic batteries face a severe self-discharge issue resulting from the dissolution of the organic electrode material in the electrolyte and low electron conductivity owing to their insulating properties, which eventually results in defects such as capacity decay for a shortened lifetime. In this study, a novel composite cathode is designed using an organic electrode material impregnated with porous carbon. Poly(2,2,6,6-tetramethylpiperidinyloxy-4-yl vinylether) (PTVE) is selected as the organic electrode material, which is synthesized via radical polymerization and embedded into spherical porous graphitic carbon (GC). The PTVE-GC composite electrode achieves a high discharge capacity of 120.1 mAh g^{-1} and maintains an excellent cycling stability with a capacity retention of 87.3% after 500 cycles. In addition, the capacity remains 96.9 mAh g^{-1} at a high current density (10 C, 6 min charge) due to rapid electron transfer and the inhibition of PTVE dissolution. Therefore, the designed composite structure of the organic electrode materials and porous GC could provide guidance for the construction of high-performance electrodes for organic rechargeable batteries.

Keywords: lithium-ion batteries; organic cathode; porous carbon; radical polymers; rate capability

1. Introduction

Rechargeable batteries are commonly used in energy storage devices, thus enabling their reusability for repeated charging and discharging cycles [1]. Among rechargeable batteries, lithium-ion batteries have the widest applications ranging from small electronic devices to large-scale devices, such as transportation vehicles and energy storage systems [2, 3]. However, they have certain drawbacks, such as short lifespans, poor rate capabilities, and high costs owing to the use of expensive metals such as cobalt, nickel, and lithium [4–6]. To overcome the limitations of the high energy density of lithium-ion

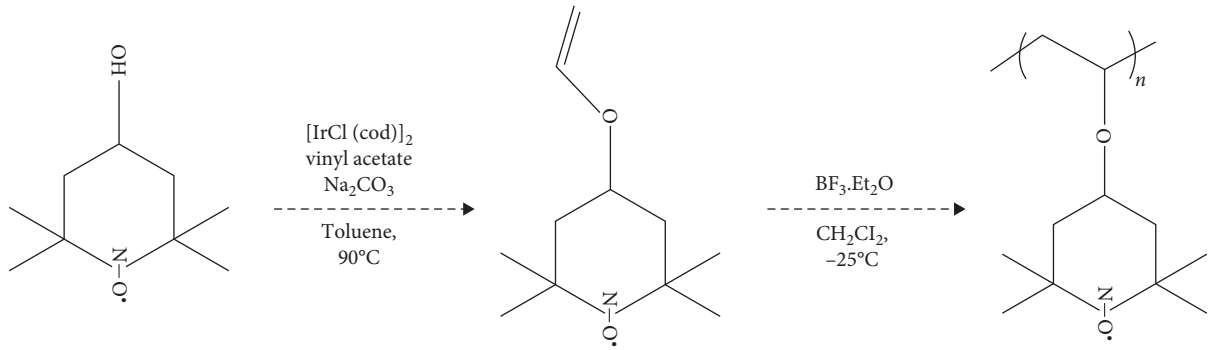

FIGURE 1: Schematic diagram of the PTVE synthesis process.

batteries, various next-generation secondary batteries, including sodium-ion, lithium-sulfur, and lithium-air batteries, have been investigated. Among them, organic polymer-based rechargeable batteries that operate via ion interactions and exhibit rapid electrochemical reaction rates have attracted significant attention [7–15].

Rechargeable organic batteries use diverse organic molecular structures as electrode materials, which are environmentally friendly and metal-free, thereby significantly reducing cell cost. Additionally, rechargeable organic batteries exhibit excellent rate capability and high power output owing to the rapid ion transfer rate and minimal volume change of the electrodes, which contribute to their superior lifespan [15–17]. The theoretical capacity of organic electrodes varies inversely with molecular weight (Mw), while the voltage plateau is dependent on atomic bonding, such as O–Li, N–O–C, or nitroxyl radical bonds, which have average voltages of <2.0, <3.0, and >3 V, respectively [18]. Regarding voltage, nitroxyl radical electrode materials are excellent at obtaining a high energy density. Nitroxyl radical electrode materials have a 2,2,6,6-tetramethyl-1-piperidinyloxy (TEMPO) pendant that comprises a nitroxyl radical (N–O•) via single bonding. The nitroxyl radical is converted to an oxoammonium cation via double bonding between nitrogen and oxygen, where the nitroxyl radical creates one electron with anion interaction in the 3.0–4.0 V range [19–21].

However, rechargeable organic batteries have drawbacks such as the ability of organic electrode materials to dissolve in liquid electrolytes, self-discharge, and capacity decay. Additionally, owing to the characteristics of the polymer materials, their actual cell capacities are lower than the theoretically achievable capacities because of their low electrical conductivities [12, 16, 18]. To address the issues of solubility and low electrical conductivity of organic electrode materials, our proposed method involves incorporating organic active materials into porous carbon structures to fabricate electrode materials with superior electrical conductivity [16, 18].

In this study, a poly(2,2,6,6-tetramethylpiperidinyloxy-4-yl vinylether) (PTVE) organic polymer material was synthesized, employed as an cathode, and incorporated into porous graphitic carbon (GC) structures with excellent electrical conductivity to fabricate the PTVE-GC (28 wt.% GC and 72 wt.% PTVE) organic electrode material. Porous carbon, rich in crystalline carbon, contain numerous pores categorized as micropores (<2 nm), mesopores (2–50 nm), and macropores (>50 nm) based on their size [14, 22, 23]. To characterize the battery, an organic electrode was prepared using the doctor blade method with a loading quantity of 4.2 mg cm^{-2}. The organic battery exhibited a high discharge capacity of 134.7 mAh g^{-1}, which corresponded to 99.7% of the theoretical capacity, at a current density of 0.3C with excellent cycling performance.

2. Experimental

2.1. Materials. To synthesize the PTVE organic electrode material, the $IrCl(cod)_2$ (Sigma-Aldrich) catalyst was used to promote the efficient dispersion of vinyl acetate. Sodium carbonate (Na_2CO_3, Sigma-Aldrich) was used to facilitate the hydrogen detachment from 4-hydroxy-2,2,6,6-tetramethylpiperidine-1-oxyl (TEMPO-OH). The initial materials comprised TEMPO-OH (Sigma-Aldrich) and vinyl acetate (Sigma-Aldrich), while anhydrous toluene (Sigma-Aldrich) was used as the solvent. BF_3•Et_2O (Sigma-Aldrich) was used as the catalyst and dichloromethane (Sigma-Aldrich) served as the solvent for polymerization. Methanol, hexane, and ether (all from Sigma-Aldrich) were used as supporting information. The average Mw of synthesized PTVE was 14,300.

2.2. Synthesis of PTVE. The synthesis of the PTVE organic polymer electrode material involved two steps: monomer synthesis and polymerization [24]. Figure 1 illustrates the first step of the PTVE monomer synthesis process. The reaction mixture was prepared by adding $IrCl(cod)_2$, 4-hydroxy-TEMPO, and Na_2CO_3 under an Ar atmosphere. The mixture was continuously stirred with the addition of anhydrous toluene and vinyl acetate. During the polymerization reaction, the monomer obtained from the first step was evaporated again and placed in a low-temperature reaction vessel maintained at −25°C under an Ar atmosphere. CH_2Cl_2 and BF_3•Et_2O were then added. After homogeneous mixing, methanol was added under stirring to dissolve the solidified reaction products. The solvent was removed from the concentrate, and ether was added while stirring. The mixture was subjected to repetitive ether–hexane–ether extraction for crystallization to obtain PTVE.

2.3. Preparation of Porous GC. Porous GC, which served as the host material for the PTVE, was synthesized using an aerosol-based spray pyrolysis method [10, 25]. A mixture of

polyvinylpyrrolidone, polystyrene nanobeads ($\phi = 100$ nm), and iron(III) nitrate nonahydrate was prepared in an H_2O solvent. The mixture underwent aerosol synthesis at 700°C under a nitrogen atmosphere with a nitrogen flow rate of 10 L min^{-1}. The intermediate product obtained during this process was further subjected to a reduction heat treatment at 600°C for 3 h under an H_2/Ar atmosphere. The resulting mixture containing iron was stirred at a 1:1 vol.% ratio of distilled water and hydrochloric acid for 48 h and washed thrice with distilled water, followed by centrifugation to obtain the final porous GC powder. The spray pyrolysis process involved a droplet generator, high-temperature furnace where drying and pyrolysis of the droplets occurred, and bag filter for powder recovery [25]. Spray pyrolysis offers advantages such as fast synthesis time and simplicity of operation. To impregnate PTVE into the porous GC structure, the two were mixed in a ratio of 28:72 wt.% and then mixed in a solvent mixture of 1-methyl-2-pyrrolidone (NMP) and acetone (volume ratio, 1:2). The mixture was evaporated using a rotary evaporator for 3 h to obtain a PTVE-porous GC composite powder.

2.4. Structural Characterization. Surface observations of the organic PTVE electrode material were performed using a scanning electron microscope (SEM) (Nanonova 230, FEI), while the organic composite electrode material was observed using transmission electron microscopy (TEM, JEM-3010 JEOL). Elemental distributions on the surface were confirmed using energy-dispersive X-ray spectrometry (EDS) mapping, and atomic distributions were analyzed using TEM-EDS. Fourier transform infrared (FTIR) spectroscopy (IFS 66/S Bruker Optik GmbH) was used to analyze the molecular structure, composition, and functional groups of the samples. The radical formation of the synthesized polymers was analyzed using electron spin resonance (ESR, JES-FR30, JEOL). The specific surface area and pore size distribution were determined using Brunauer–Emmett–Teller (BET) analysis (ASAP 2010) using nitrogen gas as the adsorbent. To measure the carbon content within the system, thermogravimetric analysis (TGA, D-TGA, SDT 2960) was conducted under an Ar atmosphere at a heating rate of 5°C min^{-1} up to 600°C. X-ray photoelectron spectroscopy (XPS, PHI 5500, ULVAC-PHI) was employed to analyze the structural characteristics of carbon. Electrical conductivities of electrodes were measured at a current value of 5 μA through the hall effect using the 4-point probe method (CMT-SR3000S). Ab initio Hartree–Fock (HF) self-consistent field (SCF) molecular orbital calculations have been performed for the lowest unoccupied molecular orbital (LUMO) and the highest occupied molecular orbital (HOMO) of PTVE using the standard 6-31G* basis set.

2.5. Electrochemical Characterization. To analyze the electrochemical properties, electrodes were fabricated using a PTVE-porous GC composite as the cathode material. For electrode fabrication, a slurry was prepared by dispersing the PTVE-GC active material, Super P carbon black (conductive additive), and a polyvinylidene fluoride (PVdF) binder in a weight ratio of 80:10:10 in an NMP solvent. The slurry was coated on aluminum foil using a doctor-blade, followed by vacuum drying in an oven at 90°C for 12 h to fabricate the cathode. A coin-type cell (CR2032) was assembled by stacking the cathode with lithium metal as the reference electrode with a thickness of 100 μm, and Celgard-2200 polyethylene was used as the separator. A carbonate-based liquid electrolyte was prepared by dissolving 1 M of $LiPF_6$ salt in a mixture of ethylene carbonate and diethyl carbonate in a 1:1 volume ratio. Charge–discharge measurements were performed using a WBCS3000 battery cycler in the voltage range of 3.0–4.0 V at various current densities (0.3, 0.8, 1.5, 5, and 10C) and at 25°C. Electrochemical impedance spectroscopy (EIS, IM6 impedance analyzer 100–2 MHz) was performed in the frequency range of 0.01 Hz to 100 kHz after the cells rested for 24 h.

3. Result and Discussion

3.1. Characterization of PTVE and PTVE-GC Composites. The morphology of the PTVE that was synthesized via radical polymerization is shown in Figure S1. In free-radical polymerization, radicals generated from initiators participate in a polymerization reaction to form a polymer under specific conditions. Figure S1 shows that the PTVE particles exhibited typical polymer characteristics with varying sizes and irregular shapes, ranging from 1 to 3 μm. The FT-IR spectrum in Figure 2a shows absorption peaks at 2933, 2869, 1463, and 1361 cm^{-1}, which corresponded to the C–H stretching vibrations of the methyl (–CH_3) and methylene (–CH_2) groups in the hydrocarbon moiety of TEMPO. The peaks at 1037 and 1307 cm^{-1} were attributed to the C–O and C–N vibrations of PTVE, respectively. The peaks at 3500 and 1234 cm^{-1} corresponded to N–H and C–O–C stretching vibrations, respectively. The stretching motions of C–O–C, the major molecular structure of PTVE, and N–O•, which directly participated in the electrochemical reactions of the organic electrode material, were observed at 1241 and 1363 cm^{-1}, respectively, thus indicating the successful synthesis of PTVE without significant changes to the initial material. The NMR spectra of PTVE were comprehensively analyzed using ^{1}H NMR and ^{13}C NMR, as depicted in Figure S2. The ^{1}H NMR spectrum offers valuable insights into the local chemical environments of hydrogen atoms. The multiplet at δ 3.85 ppm is attributed to a methine (–CH–) proton positioned adjacent to the nitroxyl radical (–N–O•). Moreover, the sharp singlet at δ 1.11 ppm suggests the presence of symmetrically arranged methyl groups, characteristic of a tert-butyl moiety, reinforcing the well-defined molecular structure of PTVE. The ^{13}C NMR spectrum provides further elucidation of the electronic environments of the carbon skeleton. The distinct resonances at δ 75.6 and 74.8 ppm correspond to C–O or C–N bonds, which are strongly associated with the nitroxyl radical (–N–O•) functionality. These well-resolved spectral signatures confirm the anticipated molecular architecture of PTVE, verifying its successful synthesis with a structurally intact polymer backbone and a stable radical functionality. Figure 2b shows the generation and concentration of free radicals using ESR analysis. 4-Hydroxy-TEMPO contains a free radical, and the synthesized PTVE also contained an N–O• free radical. If each TEMPO molecule contained one nitroxyl radical, the relative radical concentration could be

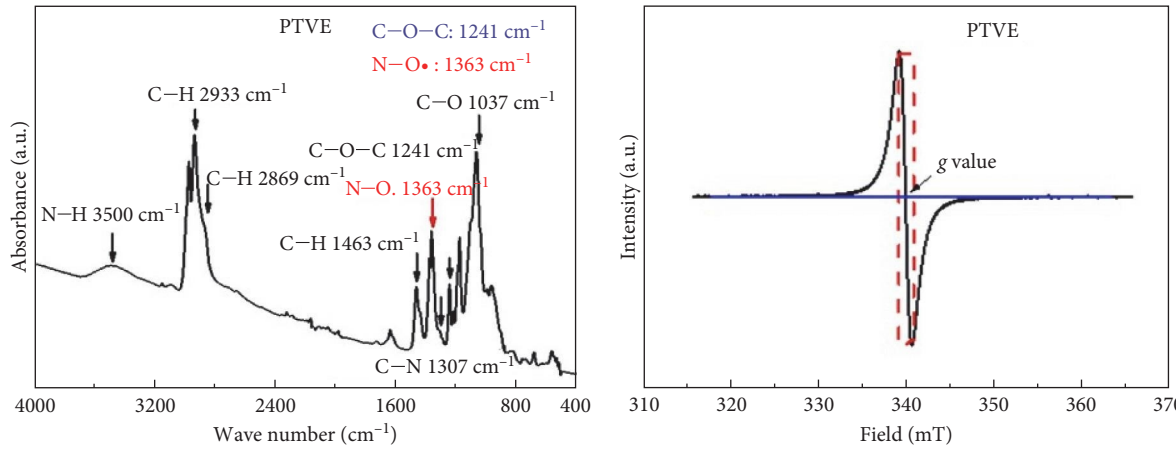

FIGURE 2: (a) FT-IR and (b) ESR curves of the synthesized PTVE powder.

estimated. The hyperfine splitting of PTVE shown in Figure 2b occurred at a g value of 2.005, indicating that 99.9% of the radicals were due to the unpaired electrons of oxygen. The LUMO and HOMO energy of PTVE calculated by DFT was −8.17 and −9.98 eV (Figure S3). The graphitic degree of a carbon can be characterized by the intensity ratio of the D-band and the G-band ($R = I_D/I_G$). A higher R value means more defects in the crystal, and a lower R value is high graphitization. Two spectra appear at 1348.7 cm^{-1} in the D-band and 1583.2 cm^{-1} in the G-band (Figure S4). The R value of porous GC is 0.92 and indicates high graphitic structure carbon of high electrical conductivity.

Figure 3a–c presents the SEM images of the spherical porous carbon structure prepared via spray pyrolysis. The size distribution of the spherical porous carbon ranged from 1 to 3 μm, with an average particle size of 1.5 μm. The cellular surface morphology analysis of the particles revealed the presence of numerous pores, the sizes of which were consistent with a diameter of 50 nm, thereby offering suitable space for accommodating PTVE. Figure 3d shows the BET results of the N_2 gas adsorption–desorption isotherms, which demonstrated the typical hysteresis phenomenon observed in porous materials. The specific surface area of the porous carbon was 400 $m^2\,g^{-1}$, determined by analyzing the gas adsorption capacity on the surface with BET, indicating the presence of well-formed pores on the particle surface. Figure 3e,f shows the morphology of the composite electrode, where PTVE was encapsulated within the porous carbon structure. Even after encapsulation, the spherical carbon encapsulant retained its particle size and exhibited well-defined cellular-like pores on its rough surface. This indicated that PTVE did not cover the surface of the porous carbon but instead effectively filled the interior pores [26]. To analyze the filled PTVE, SEM-EDS characterization was performed. Figure 3g reveals that carbon, the primary constituent of both the carbon structure and PTVE, was widely distributed. Conversely, oxygen and nitrogen, which constituted a small portion of the PTVE molecular structure, displayed low dispersion densities (Figure S5). Although their concentrations were lower than that of carbon, the presence of oxygen and nitrogen atoms in PTVE coincided with the location of the pores, indicating that PTVE filled the interior of the pores. Figure 3h shows the N_2 gas adsorption–desorption isotherm of PTVE-GC with a specific surface area of 12 $m^2\,g^{-1}$. This suggested that as an organic electrode material, PTVE was well encapsulated within the porous carbon structure, which significantly reduced the specific surface area. Because these pores were filled with PTVE, the organic electrode material was less prone to dissolve into the electrolyte during the charging–discharging process.

To further examine PTVE in porous carbon, TEM characterization was conducted to observe the morphology of pure porous GC and PTVE-impregnated GC, as shown in Figure 4. Figure 4a,b shows the vacant regions inside the pure porous carbon structure, which appeared bright gray because PTVE was not encapsulated within them. However, the PTVE-encapsulated structure in Figure 4d,e appeared darker than the pure porous carbon structure. Moreover, the surface was rough, with the outer portion appearing bright gray and the interior appearing dark black, indicating the presence of the filling material. TEM mappings (Figure S6a,b) revealed the presence of carbon and oxygen as the constituent elements, and the concentration of the primary constituent, carbon, was higher. However, oxygen, which is a component of PTVE, was evenly distributed within the particles, suggesting that PTVE filled the interior of the porous carbon structure. By effectively filling the carbon structure, the organic composite electrode material improved electron transfer during electrochemical reactions and suppressed the dissolution of organic materials, thus preventing self-discharge of the cells. TGA was performed to evaluate the PTVE content of the porous carbon structure. Figure 4c shows the TGA curve of pure PTVE, where PTVE started to decompose at ~250°C, following a rapid weight decrease. When the temperature increased to 500°C, the remaining weight ratio of 7% represented the residual carbon material following complete decomposition of the PTVE polymer. Regarding PTVE-impregnated GC (Figure 4f), the decomposition temperature of PTVE in the PTVE-porous carbon composite was ~300°C. This result suggested that encapsulating the polymer within the porous carbon structure

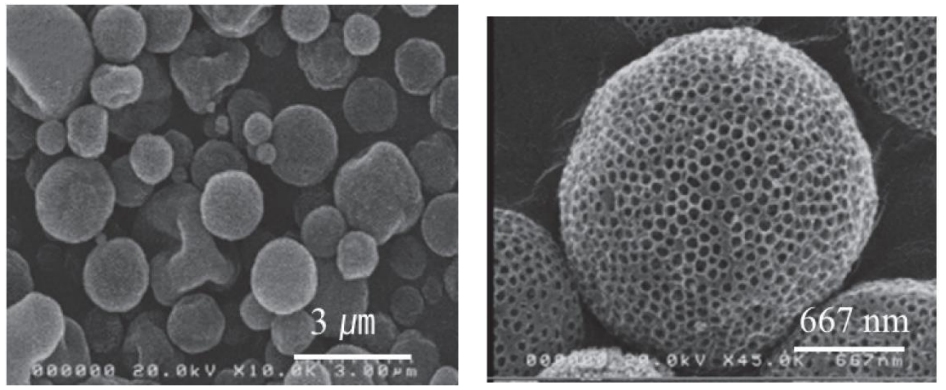

(a) (b)

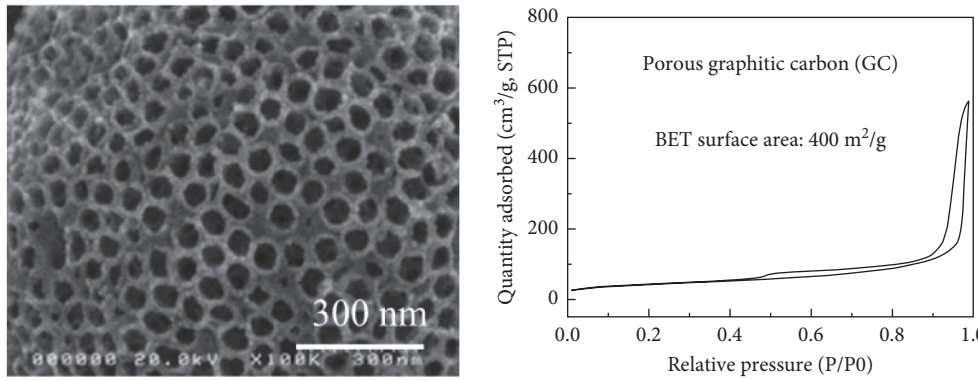

(c) (d)

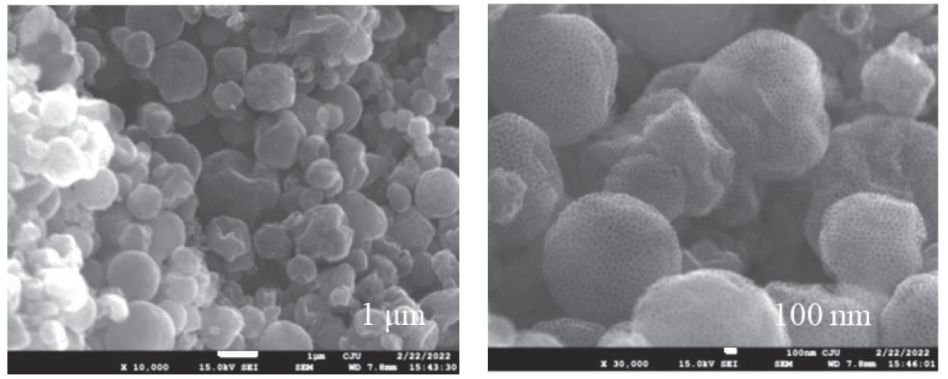

(e) (f)

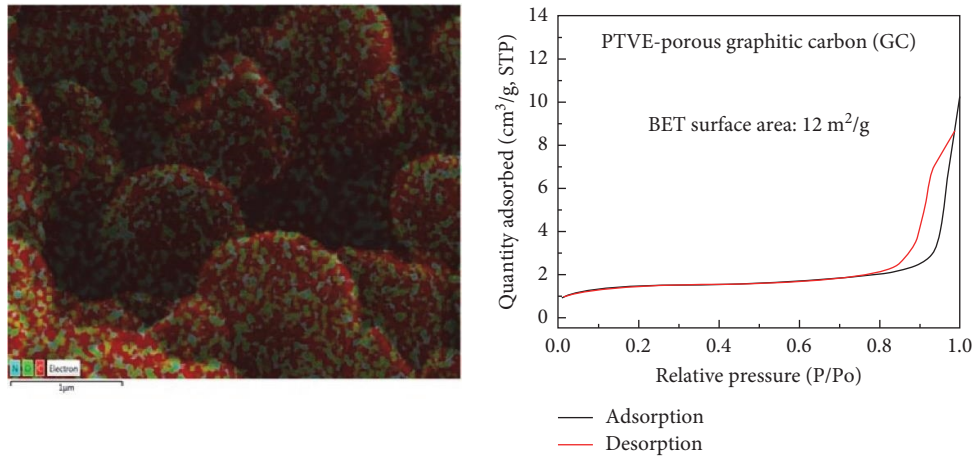

(g) (h)

FIGURE 3: (a–c) SEM images and (d) BET curve of pure porous GC. (e, f) SEM images, (g) SEM-EDS (N, O, and C atoms), and (h) BET curve of PTVE-GC.

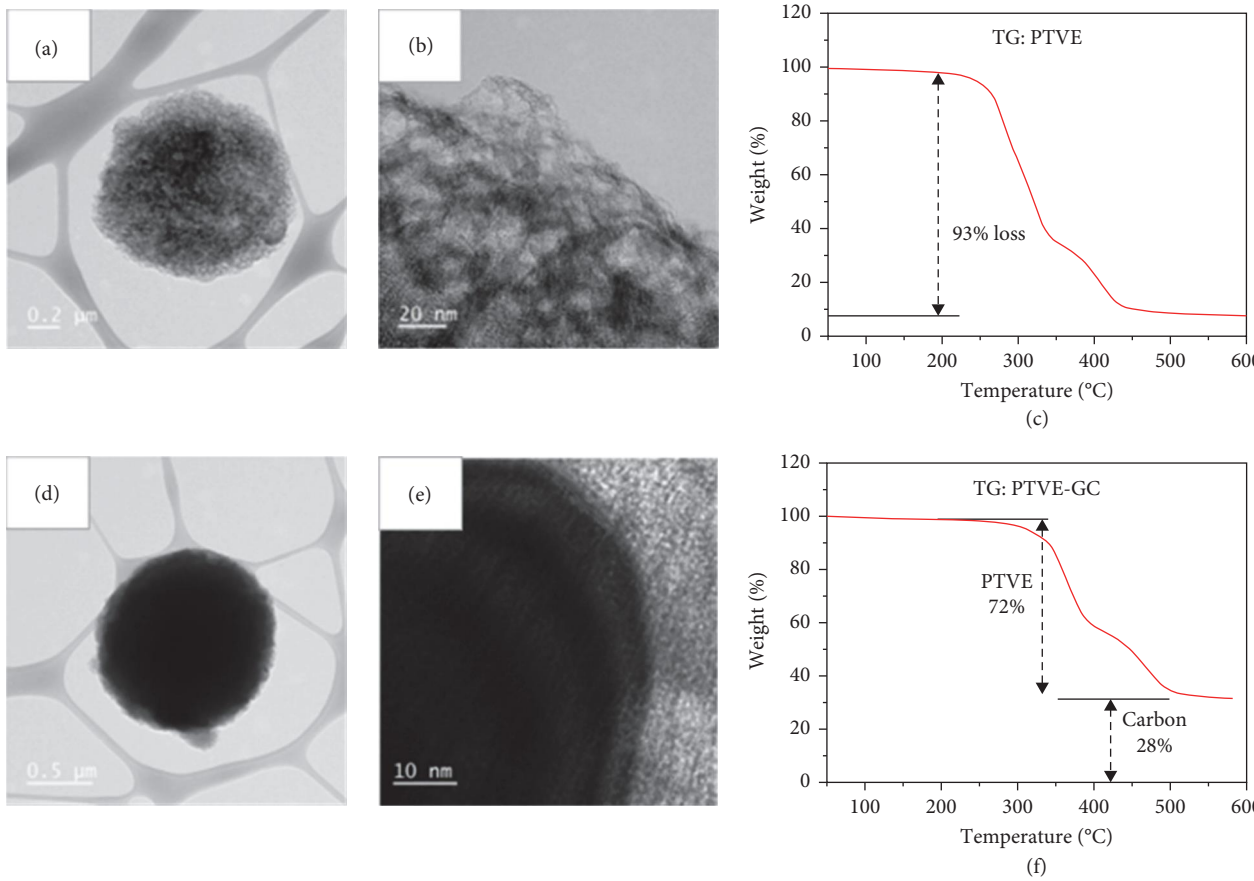

FIGURE 4: (a, b) TEM images of porous GC and (c) TGA curve of bare PTVE. (d, e) TEM images and (f) TGA curves of PTVE-GC.

enhanced the thermal stability of the PTVE. The PTVE-impregnated GC composite exhibited a weight loss ratio of 72% after 500°C, with the remaining 28% of the weight representing the carbon content. Among the 28% carbon, 5% corresponded to carbon transformed from PTVE, resulting in a PTVE content of 72% in the PTVE-porous carbon composite structure. XPS provided insights into the chemical characteristics of the PTVE-GC composite electrode surface. Figure S7a shows the overall elemental spectrum, in which the C 1s, O 1s, and N 1s species were the dominant constituent elements of the PTVE-GC composite structure. Figure S7b presents a detailed C 1s spectrum, demonstrating the presence of C—C (sp^2 and sp^3) bonds in the carbon structure, as well as C—O and C═O bonds. The separated peaks in the spectrum indicated that a higher ratio of sp^2 in the carbon material corresponded to a higher content of graphite-like structures, resulting in increased electron conductivity. In the synthesized PTVE-GC composite structure, the sp^2 structure was more than four times higher than that of sp^3, rendering the porous carbon beneficial for enhancing the electrochemical properties of organic rechargeable batteries [27, 28]. Figure S8 shows a detailed N 1s and O 1s spectrums. The nitroxide radical is displayed in 400–402 eV of N 1s and 532 eV of O 1s spectras. The nitroxide radical (N–O·) in the synthesized PTVE is oxidized to an oxoammonium cation (+N═O) during charging process.

3.2. Electrochemical Performance of PTVE and PTVE-GC Cells. The pure porous GC and PTVE-impregnated GC electrodes were evaluated, and their electrochemical performances were compared (Figure 5). Figure S9 compares the CV curves of the bare PTVE and PTVE-GC cathodes. A single pair of well-defined redox peaks in both cells is observed. The smaller gap of oxidation–reduction peaks of PTVE-GC shows the efficient and fast redox reactions occurring at the nitroxide radical site. PTVE undergoes a distinctive reversible redox process involving nitroxide radicals in the TEMPO pendant. During charging, the nitroxide radical in the synthesized PTVE is oxidized to an oxoammonium cation, releasing one electron. The emitted electrons are rapidly transferred through the porous GC. This behavior is characteristic of p-type materials, which, in this study, interact with PF^{6-} anions. In the discharge process, the oxoammonium cation is reduced, regenerating the nitroxide radical. The incoming electrons are transferred to TEMPO through heterogeneous electron transfer from GC. The TEMPO pendant transfers electron to neighboring oxoammonium cations by homoguous self-exchange electron transfer, and the electrochemical reduction reaction is rapidly transferred [24, 29]. The PTVE content of the PTVE-GC electrode was ~58 wt.%. For a comparative analysis of the PTVE batteries, the compared electrodes were manufactured with the same cell configuration using 58, 32,

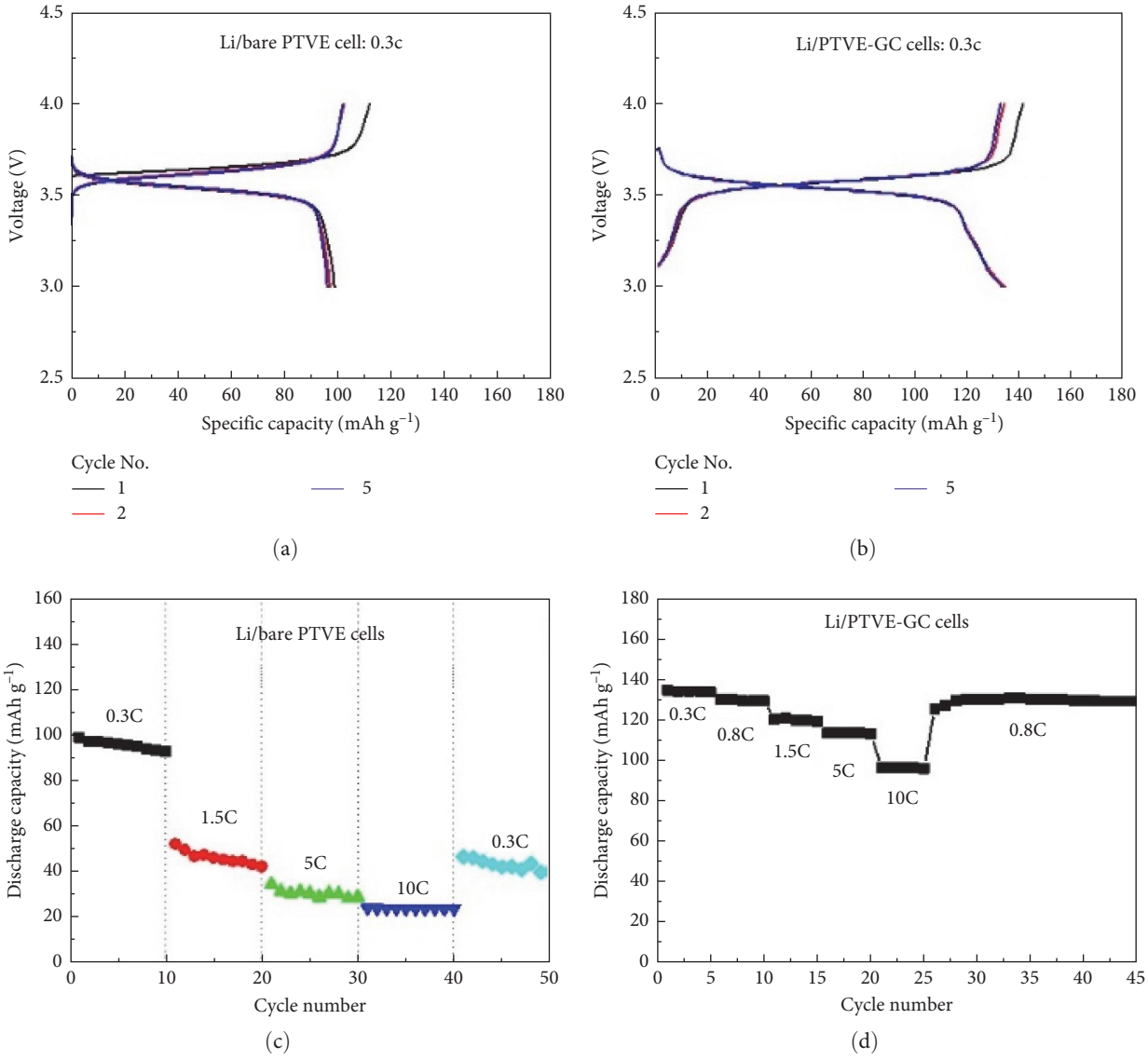

FIGURE 5: Selected charge–discharge curves of the (a) bare PTVE electrode and (b) PTVE-impregnated GC. Rate capabilities of the (c) bare PTVE and (d) PTVE-GC cells.

and 10 wt.% PTVE, Super P carbon black, and PVdF binder, respectively. The electrical conductivities of PTVE and PTVE-GC electrodes were 4.5×10^{-4} S cm^{-1} and 7.8×10^{-3} S cm^{-1}. In Figure 5a,b, the pure PTVE electrode demonstrated a low discharge capacity of 99 mAh g^{-1} and an initial Coulombic efficiency of 88.3% at 0.3C. In contrast, the PTVE-GC battery exhibited a significantly higher first-cycle discharge capacity of 134.7 mAh g^{-1}, with an improved initial Coulombic efficiency of 95.0%. Additionally, a lower polarization was observed in the PTVE-impregnated GC than in the bare PTVE cell, which indicated a significant increase in internal resistance. This occurred probably due to the PTVE coating on the carbon conductive agent prepared by simple mixing, thus hindering rapid electron transfer in the electrode [30, 31]. The electrode-based energy densities of pure PTVE and PTVE-GC cells were 348 and 483 Wh kg^{-1}, respectively. When the cells underwent several cycles, degradation in the discharge capacity was detected for the bare PTVE cell, whereas a high coincidence was observed in the PTVE-impregnated GC cell, suggesting that a more stabilized solid electrolyte interphase was formed [32]. The rate capabilities of both the electrodes were evaluated (Figure 5c,d). The bare PTVE cell exhibited rapid capacity decay at a low current of 0.3C. When the current densities increased to 1.5, 5, and 1C, the capacities decreased to 52.3, 34.5, and 24.1 mAh g^{-1}, respectively, exhibiting the extremely poor rate capacity of the bare PTVE electrode. Even though the current density returned to 0.3C to evaluate the cell recovery capability, only 47% of the initial capacity was recovered. By contrast, the PTVE-impregnated GC electrode exhibited capacities of 120.1, 113.8, and 96.9 mAh g^{-1} at 1.5, 5, and 10C, respectively. These results demonstrated the excellent rate capability of the PTVE-GC electrode, which achieved a discharge capacity that was 71.8% of the theoretical capacity at a fast-charging rate (10C) after 6 min. Additionally, the cell

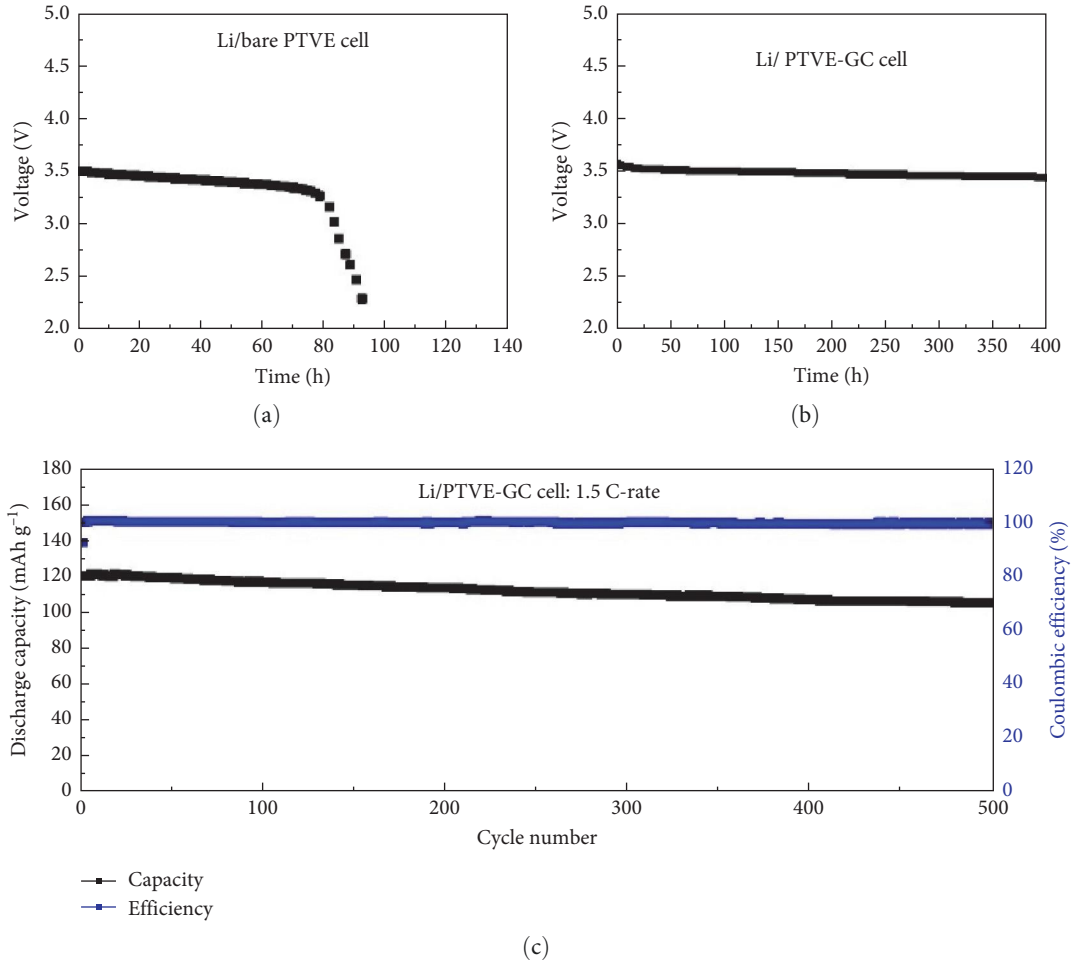

FIGURE 6: Self-discharge tests of the (a) bare PTVE and (b) PTVE-impregnated carbon cells. (c) Long-term cycling performance of the Li/PTVE-GC cell at 1.5C.

exhibited outstanding restorability (capacity recovery attained 96.5%) when the current density was reduced back to 0.8C after 10C. The results indicate that in the bare PTVE cell, Super P, used as a carbon conductive agent, is merely physically mixed with PTVE without forming a protective layer. Consequently, the low conductivity and high solubility of PTVE remain unresolved, leading to poor electrochemical performance. In contrast, in the PTVE-GC structure, PTVE is encapsulated within the pores of GC. This encapsulation suggests that GC, serving as a protective barrier, not only enhances conductivity but also effectively prevents the dissolution of PTVE. As a result, even after undergoing rigorous rate tests, the PTVE-GC structure maintains a high and stable electrochemical capacity when the cell returns to a lower rate. EIS revealed a lower resistance of the PTVE-impregnated GC (Figure S10), indicating that incorporating PTVE into the porous carbon structure improved ion-transport and electron transfer. Chen et. al. [33] studied the anticorrosion performance by a Bode-phase diagram. The diagram is useful to evaluate electrochemical kinetics of PTVE electrodes. The PTVE-GC electrode has higher reaction kinetic. In Figure S11, PTVE and PTVE-GC cells present the single steps of GITT. ΔEt and ΔEs show the change in the cell voltage during the charging. The voltage changes from the steps are recorded as a function of time, and the lithium diffusion coefficient was calculated using the Fick's second law equation [34]. The lithium diffusion coefficient is proportional to ΔEs and PTVE-GC cell is higher than PTVE. The change of surface atoms bonding of PTVE-GC electrodes was analyzed by XPS (Figure S12). The peaks at 395–404 eV for N 1s are from the TEMPO-based nitroxide radical of PTVE and ~400 eV peak of N-O• is shifted to 402 eV of N═O during charging process of PTVE-GC cell [35]. It returns to ~400 eV with discharge. The TEMPO-based nitroxide radical (N–O•) of initial state is oxidized to an oxoammonium cation (N═O+) during charging. During discharging, the oxoammonium cation is back to a nitroxide radical with reduction.

To analyze the self-discharge characteristics, pure PTVE and PTVE-GC cells were charged and allowed to rest over time. As shown in Figure 6a, the pure PTVE organic battery exhibited a gradual decrease in voltage over time, followed by a rapid decrease after 80 h. This indicated that self-discharge was accelerated when a certain amount of PTVE was dissolved in the electrolyte. In contrast, Figure 6b shows that the PTVE-GC cell maintained a stable voltage without significant changes for up to 400 h. This suggested that the PTVE embedded within

the porous carbon structure inhibited its dissolution into the electrolyte, thus preventing self-discharge of the cells. Figure 6c shows the long-term cycling performance of the PTVE-GC cell. The initial discharge capacity was 120.1 mAh g^{-1}, and it maintained remarkable cycling stability with a capacity retention of 87.3%. After 500 cycles, the capacity decay per cycle maintained an extremely low value of 0.03 mAh g^{-1}. Additionally, the average Coulombic efficiency remained >99% for up to 500 cycles. The electrochemical performance of PTVE-GC exceeds the previously reported electrochemical performance of organic material/carbon composite-based cathodes, as shown in Table S1. These excellent electrochemical performances indicate that the structure of the PTVE-GC composite electrode can play a promising role in overcoming the drawbacks of organic batteries.

3.3. Discussion. The exceptional electrochemical performance of the PTVE-GC composite battery stems from the synergistic interplay between the redox-active PTVE polymer and the highly conductive, porous GC framework. The remarkably high discharge capacity and superior rate capability suggest that the PTVE polymer undergoes highly efficient and reversible redox reactions, facilitated by the intrinsic conductivity and interconnected pore network of the GC matrix, which ensures rapid electron and ion transport. Furthermore, the robust interfacial interaction between the PTVE-GC composite particles and the aluminum current collector plays a pivotal role in maintaining stable long-term cycling performance. This intimate contact not only enhances charge transfer kinetics but also suppresses active material dissolution, thereby mitigating self-discharge and minimizing capacity fading. The remarkable capacity retention of 87.3% after 500 cycles further underscores the structural integrity and electrochemical durability of the composite material, which is critical for the practical implementation of organic secondary batteries. These findings demonstrate that the PTVE-GC composite electrode effectively addresses fundamental challenges associated with organic batteries, including intrinsically low electronic conductivity, active material solubility, and self-discharge phenomena. The strategic integration of a redox-active polymer with a conductive, porous scaffold offers a highly promising pathway toward next-generation, high-performance organic energy storage systems with enhanced stability, efficiency, and longevity.

4. Conclusion

The PTVE polymer was successfully synthesized via radical polymerization and verified to contain high-purity nitroxyl radicals through comprehensive NMR, FT-IR, and ESR analyses. Morphological and structural characterization using SEM, TEM, and TGA confirmed that 72 wt.% of PTVE was effectively confined within the porous framework of the GC structure, ensuring optimal material utilization. Electrochemical evaluation of the PTVE-GC composite electrode demonstrated an exceptional discharge capacity of 134.7 mAh g^{-1}, achieving 99.7% of its theoretical capacity at a current density of 0.3C. Moreover, the cell exhibited outstanding rate capability, retaining a discharge capacity of 96.9 mAh g^{-1} even under high-rate conditions during 6-min charging cycles. Long-term cycling stability was further evidenced by an ultralow capacity decay of 0.03 mAh g^{-1} per cycle over 500 cycles, maintaining an impressive capacity retention of 87.3%. These remarkable electrochemical properties highlight the efficacy of the PTVE-GC composite architecture, where the synergistic interplay between the highly conductive porous GC framework and redox-active PTVE polymer enables efficient charge transport, mitigates self-discharge, and suppresses active material dissolution. The exceptional stability and high-rate performance highlight the potential of this composite electrode design as a transformative approach toward next-generation, high-performance organic secondary batteries with superior durability and electrochemical efficiency.

Data Availability Statement

The data that support the findings of this study are available from the corresponding author upon reasonable request.

Conflicts of Interest

The authors declare no conflicts of interest. Ji-Won Son and Tae Ju Kang are affiliated with the Swemeka Co. Ltd.

Author Contributions

Ji-Won Son: writing – original draft, methodology, investigation, data curation. **Jae Seob Lee:** methodology, investigation, data curation. **Hyun Ho Choi:** methodology. **Hong-Il Kim:** methodology. **Shan Fang:** methodology. **Tae Ju Kang:** methodology. **Fanglin Wu:** supervision, project administration, writing – review and editing. **Hyun Woo Kim:** supervision, project administration, writing – review and editing. **Ying Liu:** writing – review and editing. **Jung Sang Cho:** supervision, project administration, writing – review and editing. Ji-Won Son and Jae Seob Lee contributed equally to this work.

Funding

This work was supported by the National Research Foundation of Korea (NRF) grant funded by the Korean government (MSIT) (No. RS-2023-00217581 and RS-2025-00556955) and Technology Development Program (No. S3310353) funded by the Ministry of SMEs and Startups.

Supporting Information

Additional supporting information can be found online in the Supporting Information section. (*Supporting Information*)
The supporting information contains detailed experimental results for this paper. It includes the following information. Table S1: Summary of previous studies on organic material/carbon composite-based cathode for LIBs/SIBs. Figure S1: SEM images of synthesized PTVE powder. Figure S2: 1H and 13C NMR spectrum of synthesized PTVE. Figure S3: DFT calculations of LUMO and HOMO for PTVE. Figure S4. Raman spectra of porous graphitic carbon (GC). Figure S5: The SEM-EDS of N and O element. Figure S6: The TEM mapping of (a) C and (b) O element. Figure S7: (a) XPS survey and (b) C1s spectrum of PTVE-impregnated graphitized carbon.

Figure S8. N 1s and O 1s spectrum of PTVE-GC. Figure S9. CV comparison of bare PTVE and PTVE-GC (room temperature, 3.0 to 4.0 V, 1 mV/s). Figure S10: EIS curves of bare PTVE cell and PTVE-impregnated porous carbon cell before cycling. Figure S11: Charge GITT curves of PTVE and PTVE-GC cells. Figure S12: Ex situ XPS spectra of the binding energy of N 1s of PTVE-GC cells before cycling, after charging and after discharging.

References

[1] J. B. Goodenough and K.-S. Park, "The Li-Ion Rechargeable Battery: A Perspective," *Journal of the American Chemical Society* 135, no. 4 (2013): 1167–1176.

[2] F. Wu, Z. Chen, S. Fang, W. Zuo, G.-T. Kim, and S. Passerini, "The Role of Ionic Liquids in Resolving the Interfacial Chemistry for (Quasi-) Solid-State Batteries," *Energy Storage Materials* 63 (2023): 103062.

[3] H. Byeon, B. Gu, H.-J. Kim, et al., "Redox Chemistry of Nitrogen-Doped CNT-Encapsulated Nitroxide Radical Polymers for High Energy Density and Rate-Capability Organic Batteries," *Chemical Engineering Journal* 413 (2021): 127402.

[4] N. Nitta, F. Wu, J. T. Lee, and G. Yushin, "Li-Ion Battery Materials: Present and Future," *Materials Today* 18, no. 5 (2015): 252–264.

[5] J.-W. Lee and W.-B. Kim, "Research Trend of Electrode Materials for Lithium Rechargeable Batteries," *Journal of Korean Powder Metallurgy Institute* 21, no. 6 (2014): 473–479.

[6] J. Mohanta, H.-J. Kim, S. M. Jeong, et al., "High-Performance Quasi-Solid-State Flexible Sodium Metal Battery: Substrate-Free FeS_2–C Composite Fibers Cathode and Polyimide Film-Stuck Sodium Metal Anode," *Chemical Engineering Journal* 391 (2020): 123510.

[7] J. W. Fergus, "Recent Developments in Cathode Materials for Lithium Ion Batteries," *Journal of Power Sources* 195, no. 4 (2010): 939–954.

[8] K. B. Hueso, M. Armand, and T. Rojo, "High Temperature Sodium Batteries: Status, Challenges and Future Trends," *Energy & Environmental Science* 6, no. 3 (2013): 734–749.

[9] J.-Y. Hwang, S.-T. Myung, and Y.-K. Sun, "Sodium-Ion Batteries: Present and Future," *Chemical Society Reviews* 46, no. 12 (2017): 3529–3614.

[10] H. Pan, Y.-S. Hu, and L. Chen, "Room-Temperature Stationary Sodium-Ion Batteries for Large-Scale Electric Energy Storage," *Energy & Environmental Science* 6, no. 8 (2013): 2338–2360.

[11] B. L. Ellis and L. F. Nazar, "Sodium and Sodium-Ion Energy Storage Batteries," *Current Opinion in Solid State and Materials Science* 16, no. 4 (2012): 168–177.

[12] J.-K. Kim, Y. J. Lim, H. Kim, G.-B. Cho, and Y. Kim, "A Hybrid Solid Electrolyte for Flexible Solid-State Sodium Batteries," *Energy & Environmental Science* 8, no. 12 (2015): 3589–3596.

[13] M. Zhao, B.-Q. Li, X.-Q. Zhang, J.-Q. Huang, and Q. Zhang, "A Perspective Toward Practical Lithium-Sulfur Batteries," *ACS Central Science* 6, no. 7 (2020): 1095–1104.

[14] R. Saroha, J. H. Oh, Y. H. Seon, et al., "Freestanding Interlayers for Li-S Batteries: Design and Synthesis of Hierarchically Porous N-Doped C Nanofibers Comprising Vanadium Nitride Quantum Dots and MOF-Derived Hollow N-Doped C Nanocages," *Journal of Materials Chemistry A* 9, no. 19 (2021): 11651–11664.

[15] Z. Song and H. Zhou, "Towards Sustainable and Versatile Energy Storage Devices: An Overview of Organic Electrode Materials," *Energy & Environmental Science* 6, no. 8 (2013): 2280–2301.

[16] M. Li, R. P. Hicks, Z. Chen, et al., "Electrolytes in Organic Batteries," *Chemical Reviews* 123, no. 4 (2023): 1712–1773.

[17] Y. Hong, J. Hu, W. Tang, et al., "A Universal Small-Molecule Organic Cathode for High-Performance Li/Na/K-Ion Batteries," *Energy Storage Materials* 52 (2022): 61–68.

[18] Y. Lu and J. Chen, "Prospects of Organic Electrode Materials for Practical Lithium Batteries," *Nature Reviews Chemistry* 4, no. 3 (2020): 127–142.

[19] J.-K. Kim, "Single- and Double-Redox Reaction of Poly (2,2,6,6-Tetramethylpiperidinyloxy-4-Vinylmethacrylate)/ Ordered Mesoporous Carbon Composite Nitroxide Radical Polymer Battery," *Journal of Power Sources* 477 (2020): 228670.

[20] J. C. Barbosa, A. Fidalgo-Marijuan, J. C. Dias, et al., "Molecular Design of Functional Polymers for Organic Radical Batteries," *Energy Storage Materials* 60 (2023): 102841.

[21] T. S. Kim, J.-E. Lim, M.-S. Oh, and J.-K. Kim, "Carbon Conductor- and Binder-Free Organic Electrode for Flexible Organic Rechargeable Batteries With High Energy Density," *Journal of Power Sources* 361 (2017): 15–20.

[22] J. Lee, J. Kim, and T. Hyeon, "Recent Progress in the Synthesis of Porous Carbon Materials," *Advanced Materials* 18, no. 16 (2006): 2073–2094.

[23] S. H. Yang, J. M. Choi, R. Saroha, S. W. Cho, Y. C. Kang, and J. S. Cho, "Hollow Porous Carbon Nanospheres Containing Polar Cobalt Sulfide (Co_9S_8) Nanocrystals as Electrocatalytic Interlayers for the Reutilization of Polysulfide in Lithium-Sulfur Batteries," *Journal of Colloid and Interface Science* 645 (2023): 33–44.

[24] M. Suguro, S. Iwasa, Y. Kusachi, Y. Morioka, and K. Nakahara, "Cationic Polymerization of Poly(vinyl ether) Bearing a TEMPO Radical: A New Cathode-Active Material for Organic Radical Batteries," *Macromolecular Rapid Communications* 28, no. 18-19 (2007): 1929–1933.

[25] S.-G. Park, "Synthesis of Metal Chalcogen Compound Nanostructures via Spray Pyrolysis Process and Application as Sodium Ion Battery Anode Material," *News & Information for Chemical Engineers* 37, no. 4 (2019): 489–494.

[26] H. W. Kim, H.-J. Kim, H. Byeon, et al., "Binder-Free Organic Cathode Based on Nitroxide Radical Polymer-Functionalized Carbon Nanotubes and Gel Polymer Electrolyte for High-Performance Sodium Organic Polymer Batteries," *Journal of Materials Chemistry A* 8, no. 35 (2020): 17980–17986.

[27] J. S. Lee, R. Saroha, and J. S. Cho, "Porous Microspheres Comprising $CoSe_2$ Nanorods Coated With N-Doped Graphitic C and Polydopamine-Derived C as Anodes for Long-Lived Na-Ion Batteries," *Nano-Micro Letters* 14, no. 1 (2022): 113.

[28] L. Chen, Z. Xu, J. Li, et al., "Modifying Graphite Oxide Nanostructures in Various Media by High-Energy Irradiation," *RSC Advances* 4, no. 2 (2014): 1025–1031.

[29] W. Guo, J. Su, Y.-H. Li, L.-J. Wan, and Y.-G. Guo, "Nitroxide Radical Polymer/Graphene Nanocomposite as an Improved Cathode Material for Rechargeable Lithium Batteries," *Electrochimica Acta* 72 (2012): 81–86.

[30] K. Oyaizu, Y. Ando, H. Konishi, and H. Nishide, "Nernstian Adsorbate-Like Bulk Layer of Organic Radical Polymers for High-Density Charge Storage Purposes," *Journal of the American Chemical Society* 130, no. 44 (2008): 14459–14461.

[31] J.-K. Kim, Y. Kim, S. Park, H. Ko, and Y. Kim, "Encapsulation of Organic Active Materials in Carbon Nanotubes for Application to High-Electrochemical-Performance Sodium Batteries," *Energy & Environmental Science* 9, no. 4 (2016): 1264–1269.

[32] S. Fang, F. Wu, S. Zhao, et al., "Adaptive Multi-Site Gradient Adsorption of Siloxane-Based Protective Layers Enable High Performance Lithium-Metal Batteries," *Advanced Energy Materials* 13, no. 46 (2023): 2302577.

[33] N. Chen, J. He, H. Xuan, et al., "Dual-Functional Polyindole/MXene Composite for Superior Proton Storage and Corrosion Protection," *Composites Part B: Engineering* 270 (2024): 111145.

[34] Y.-S. Lee and K.-S. Ryu, "Study of the Lithium Diffusion Properties and High Rate Performance of $TiNb_6O_{17}$ as an Anode in Lithium Secondary Battery," *Scientific Reports* 7, no. 1 (2017): 16617.

[35] J.-K. Kim, G. Cheruvally, J.-W. Choi, J.-H. Ahn, D. S. Choi, and C. E. Song, "Rechargeableorganic Radical Battery With Electrospun, Fibrous Membrane-Based Polymer Electrolyte," *Journal of the Electrochemical Society* 154, no. 9 (2007): A839–A843.